

# Dynamics of the solar photosphere

## I. Two-dimensional spectroscopy of mesoscale phenomena

Th. Straus<sup>1</sup> and D. Bonaccini<sup>2</sup>

<sup>1</sup> Osservatorio Astronomico di Capodimonte, Via Moiarriello 16, I-80131 Napoli, Italy

<sup>2</sup> European Southern Observatory, Karl-Schwarzschild-Str. 2, D-85748 Garching, Germany

Received 28 May 1996 / Accepted 10 October 1996

**Abstract.** We address the “mesogranulation” phenomenon by analyzing a spectral time series, taken at disk center with a two-dimensional spectroscopy device and covering a period of 4 hours. This tunable device was composed by a Fabry-Perot interferometer mounted in tandem with an Universal Birefringent Filter (UBF). We calculate spatial power spectra, spatio-temporal  $k - \omega$  power, phase difference and coherence spectra at different low photospheric levels, in order to investigate the nature of the mesoscale phenomena.

At the lowest levels, mesostructures appear as a part of an extended distribution of granular sizes without further distinction from granulation. Here, the plasma flows are driven by convection. On the other hand, a different mesoscale phenomenon emerges at levels as high as approximately 200-300 km above  $\tau_{5000} = 1$ , at medium spatial ( $k \approx 0.5 \dots 2 \text{ Mm}^{-1}$ ) and medium temporal ( $\nu \approx 0.5 \dots 1 \text{ mHz}$ ) frequencies. This phenomenon is distinct from convection by its non-convective phase difference values ( $\Phi_{v-I} \approx -30^\circ$ ,  $\Phi_{v-v} < 0^\circ$ ) and by its different propagation character (almost horizontal propagation).

By these properties, the mesoscale phenomena in the higher photosphere can be identified as *internal gravity waves* in the solar atmosphere.

**Key words:** Sun: atmosphere, granulation, photosphere, oscillations – convection – hydrodynamics

---

### 1. Introduction

Fourier analysis of one or two dimensional time series of solar intensity and (vertical) velocity data has been used for a long time to discriminate different types of wave phenomena in the solar atmosphere (see e.g. the review of Noyes 1967). Deubner (1975) has identified with this method the solar 5 minute oscillations as the evanescent residue of acoustic eigenmodes of the solar interior observed outside in the atmosphere, as predicted by Ulrich (1970) and Leibacher & Stein (1971). Since

then, the  $k - \omega$  transforms have often been used for removing the 5 minute signal or as a diagnostic tool.

Recently, this technique has also been applied to the study of the solar “mesogranulation” phenomenon (Deubner 1989; Chou et al. 1991; Hathaway et al. 1991; Straus et al. 1992, hereafter called Paper I), which was first reported by November et al. (1981) as the spatial scale of solar convection corresponding to the depth of the He I ionization zone, as first argued by Simon & Leighton (1964). The above mentioned spatio-temporal investigations do not leave any doubt about the existence of quasi-stationary patterns of intermediate scales in the solar photosphere, larger than typical granules and smaller than supergranules (for the particular case of Chou et al. this has been clearly demonstrated afterwards by Ginet & Simon 1992). The introduction of  $k - \omega$  phase difference spectra to the Fourier analysis of time series (Deubner et al. 1989; Deubner 1990) amplified the power of this diagnostic, leading to a possible further distinction of different *dynamical* phenomena in the same area of the diagnostic (i.e.  $k - \omega$ ) diagram. In order to identify the types of dynamical phenomena, it is necessary to compare the observed phase lags between the velocity and intensity signals ( $\Phi_{v-I}$ ), or between velocity signals at different heights ( $\Phi_{v-v}$ ), with the results of model calculations (Marmolino & Severino 1991; Marmolino et al. 1993; Wang et al. 1995). Investigations of “mesogranulation” revealed a vanishing phase difference  $\Phi_{v-I} \approx 0^\circ$  in the lower photosphere (C I-5380, Paper I), indicating the convective character of mesoscale flow patterns.

Unlike the well proved existence of a mesoscale pattern, its distinction from granulation has never been demonstrated by observation of a gap in the spatial power spectrum of solar convection. Rather than an independent third regime of solar convection, the mesoscale structures seem to be a part of a broad distribution of granular scales, distinguished only by a power gap at the low wavenumber side from supergranulation (Paper I).

This must be checked carefully, because a partition of the solar convection zone into three vertically distinct opacity regimes – driving three regimes with different horizontal dimensions –

does not have a firm theoretical basis due to the almost negligible contribution of He-ionization to the superadiabatic gradient. Instead, a homogeneous spectrum of convective pattern sizes – including the meso scale – is favoured by theoretical model calculations (cf. Chan et al. 1991). Further, the 3D hydrodynamical simulations emphasize that the convection is driven mainly by the cooling processes at the surface rather than by heating at the lower boundary (Nordlund & Stein 1995). A possible interpretation of convection cells of mesogranular dimensions as simply another part of an “inverse cascade” creating a great variety of horizontal sizes has been proposed by Stein & Nordlund (1989).

The most powerful tool for checking this consists of a spatio-temporal analysis of (spatially) two-dimensional spectral time series (cf. Straus 1991), due to the high statistical stability of these power spectra and the possible expansion to a full dynamical study including  $k - \omega$  phase difference spectra. This can be achieved either by scanning a two-dimensional region of the solar atmosphere with the entrance slit of a traditional spectrograph (e.g. Johannesson et al. 1992; Paper I), by scanning a wavelength region with a tunable filter (e.g. Bonaccini & Stauffer 1990), or with a two-dimensional Multichannel Subtractive Double Pass (MSDP) spectrograph (e.g. Mein 1991). Due to technical limitations in both the second spatial dimension and the choice of Fraunhofer lines, the latter is not a preferable alternative for the investigation of “mesogranulation”.

A further independent method for investigating convective flows in the solar atmosphere is based on the “local correlation technique” (November & Simon 1988) which revealed hints of horizontal flows at scales greater than a typical granular size (e.g. November et al. 1987; Simon et al. 1988; Brandt et al. 1991). Both of these methods – the full Fourier analysis of the vertical velocity including a dynamical study using  $k - \omega$  phase difference spectra, and the study of the horizontal flows using the local correlation technique – can be achieved by a *single* spectral time series with a tunable filter. A first medium period time series of this type has been reported by Bendlin et al. (1993), but has not yet been Fourier analyzed, nor can “mesogranulation” be addressed because of insufficient field of view and observation period.

In the present paper we discuss a new long term time series and address the “mesogranulation” phenomenon by a dynamical study of vertical velocities. The results of a local correlation analysis of the horizontal velocity component will be discussed in a second paper. The present data can be considered as a set of data equivalent to the one of Paper I, but based on a totally independent observation method and covering the medium and high wavenumber range of the  $k - \omega$  diagram.

## 2. Observation and data reduction

The present investigation is based upon a 4 hour time series of simultaneous, short exposure (55 msec) white light images and monochromatic filter scans of two Fraunhofer lines (C I-5380 and Fe I-5380) in a  $90'' \times 90''$  field at the center of the quiet sun.

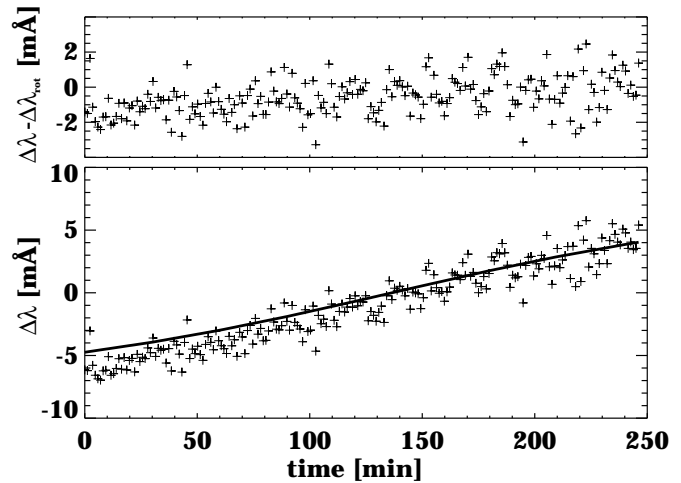


**Fig. 1.** *Lower panel:* Absolute wavelength drifts of the spectral mean profile during the 4 hours of observation (crosses). The main drift is due to the relative observer-sun velocity caused by the Earth’s rotation (solid line). Subtracting this effect leads to an approximately 1 mÅ RMS fluctuation (*upper panel*) which contains both thermal instabilities of the spectrograph system and residual global 5 min oscillations.

The observations were performed on January 31, 1993, at the VTT of the National Solar Observatory at SacPeak<sup>1</sup>, NM, using the full size of two RDA CCD cameras with  $300 \times 240$  pixels (i.e.  $0.3 \times 0.375$  / pixel) with a sampling rate of 1 frame / 2 sec. The narrow passband (30 mÅ) filtergrams were obtained by using a tunable Fabry–Perot interferometer mounted in tandem with a Universal Birefringent Filter (cf. Bonaccini et al. 1989). Each of the 212 scans of the two Fraunhofer absorption lines contains 35 single filtergrams (i.e. the scan period was 70 sec) with a step of 10 mÅ and the simultaneously taken white light images.

Dark current and flat field corrections were applied to both, the white light images and the filtergrams. The fringe patterns, present in the monochromatic filtergrams, due to interference at the optical window of the CCD, depend rather strongly on the wavelength. So, absolute wavelength drifts of the whole scan due to thermal instabilities of the Fabry–Perot filter have been taken into account for choosing the nearest flatfield image for each individual filtergram. For this, the raw filtergram data were used to determine the position of the absorption lines in the spectral mean profile giving information about the thermal drift of the Fabry–Perot during the run. Moreover, we have taken a large set of flat field images with twice the spectral resolution of the real observation in order to minimize the wavelength difference between the flat field and the image to be corrected and to keep residual noise due to flat field errors small. In this way, we were able to extend the observation up to 4 hours without interruption for further filter setup. In the whole 4 hour observ-

<sup>1</sup> Operated by the Association of Universities for Research in Astronomy, Inc., under contract with the National Science Foundation. Partial support for the National Solar Observatory is provided by the US Air Force under a Memorandum of Understanding with NSF.

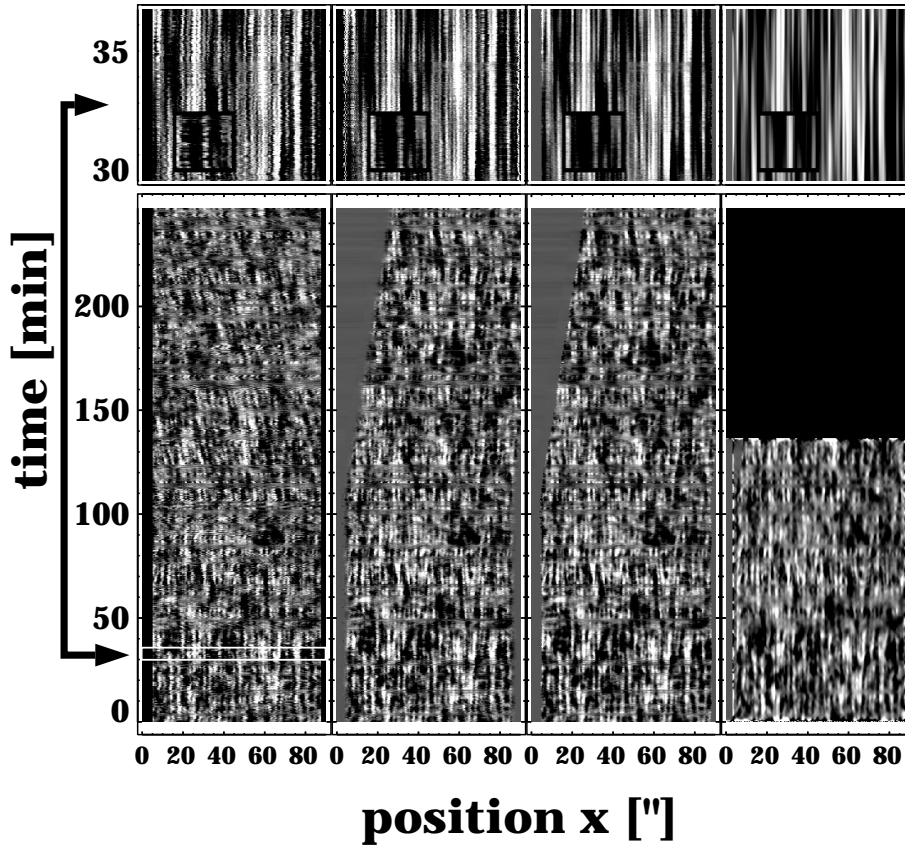


**Fig. 2a–d.** Effects of the first steps in data reduction on the time series of white light images. *Lower panels a–d* The three-dimensional data set is represented by grey scale encodings of a slice of the whole  $(x, y, t)$ -cube at the central position in  $y$ , as seen after each step of data reduction. *Upper panels A–D* Zooms into a short time interval of approx. 6 minutes, including a small further magnified region (Z), are shown for each corresponding diagram. Columns from the left to the right: a,A show the state after application of dark current and flatfield corrections; in the following diagrams global shifts (b,B), local shifts (c,C) and five-minute oscillations (d,D) have been removed, successively. In the second half of the 4 hours a systematic telescope guiding error led to the rapid loss of information on the left part of the field of view and this portion of the time series has been excluded in the last step. The five-minute oscillations were removed by applying a three-dimensional subsonic Fourier filter algorithm.

**Table 1.** Formation heights of the different levels used during data reduction (Marmolino, 1995). The values are calculated using the definition of the contribution function to the *emerging* intensity and the velocity response function, both as defined in Caccin et al. (1977).

$\frac{I-I_0}{I_{\text{cont.}}-I_0}$ [%]	C-5380Å		
	$h_I$ [km]	$h_v$ [km]	
0 (core)	30	61	
10	27	53	
30	23	41	
$\frac{I-I_0}{I_{\text{cont.}}-I_0}$ [%]	Fe-5380Å		
	0 (core)	198	265
	10	136	226
	30	88	189
	50	54	146

ing period, the Fabry–Perot filter suffered thermal instabilities corresponding to a RMS value less than about  $1 \text{ mÅ}$  or  $60 \text{ ms}^{-1}$ . For determining this value, systematic effects of the Earth’s rotation were subtracted from the absolute wavelength drifts of the mean profiles (see Fig. 1). The remaining  $60 \text{ ms}^{-1}$  signal still contains some undetermined, significant residue of global solar oscillations.

The series was analyzed for guiding errors applying a cross correlation technique to the white light images. These global drifts were then removed in both the white light images and the corresponding filtergrams. In a similar way, a Fast Fourier Transform (FFT) based *local* cross correlation algorithm (similar to the one described in November, 1989) was then used in order to determine the local spatial displacements (“stretch”) due to seeing effects. For this we compared each of the white light frames with the best of the previous ones just corrected. The correction (“destretching”) algorithm was based on bilinear interpolation and eliminated great part of the image motion (*tip-tilt*).

A summary of the results of the correction procedure is shown in Fig. 2 which represents slices  $(x-t)$  diagrams of the three-dimensional white light data cube  $I_{\text{cont.}}(x, y, t)$  at the central of the 240  $y$ -positions after each step of correction. In addition, we used the statistics of the *local* displacements determined by the destretching algorithm to estimate the quality of seeing during our observation. We, therefore, used the relation between the RMS value of the local displacements and the Fried parameter  $r_0$  given in equation (3) of Brandt et al. (1987). We should point out that we used the *spatial* statistics over the wide field of view of each white light image, rather than the *temporal* RMS fluctuations used by Brandt et al. The mean value of  $r_0$  in the whole 4 hour period amounts to approximately 12 cm.

For further investigation, a three-dimensional Fourier transformation was applied to the subset of the first 4096 white light

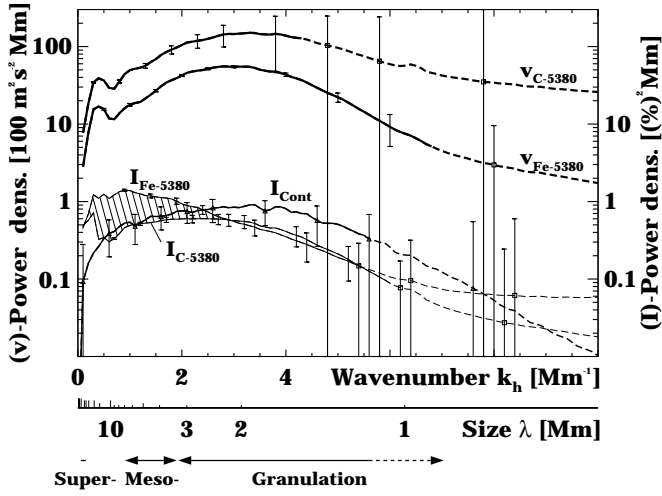


**Fig. 3.** Summary of the spatial power spectral density of the continuum intensity ( $I_{\text{cont.}}$ ), and the velocity ( $v_{\text{C-5380}}$ ,  $v_{\text{Fe-5380}}$ ) and intensity signals ( $I_{\text{C-5380}}$ ,  $I_{\text{Fe-5380}}$ ) in the line cores of both absorption lines observed. The values are represented by dashed lines where the error exceeds the observed value. The hatched region marks the power enhancement discussed in Sect. 3.1.

images (corresponding to 2.6 hours or approximately 2 Gbytes of floating point data) and the oscillation signal was removed by a subsonic filter in the  $(k_x, k_y, \omega)$  domain. A mean spatial power spectrum

$$P_{\text{cont.}} = \left\langle \sum_{k_x^2 + k_y^2 = k_h^2} T_{\text{cont.}} T_{\text{cont.}}^*(k_x, k_y, t) \right\rangle_t \quad (1)$$

was calculated from both the spatial Fourier transforms  $T_{\text{cont.}}(k_x, k_y, t)$  of all oscillation free white light images, and for a subset of the 100 images with highest contrast. The latter subset has a mean value of  $r_0$  of about 27 cm.

Independently, from each scan of the corrected filtergram data, spectral profiles were reconstructed in each spatial position  $(x, y)$  and the core intensities  $I(x, y, t)$  and Doppler velocities  $v(x, y, t)$  were determined for both Fraunhofer lines calculating the minimum position of a 2<sup>nd</sup> order polynomial fit to the line core. The intensity signal was defined by the relative core intensity fluctuations  $(I(x, y, t) - \langle I(t) \rangle) / \langle I(t) \rangle$ , and the velocity signal by the dopplershifts relative to the position of the whole fields mean profile. Additional information has been derived from the bisectors calculated at several fixed levels in the absorption lines applying a linear interpolation to the wings. An estimation of the formation heights of the velocity and intensity signals at all levels is summarized in Table 1.

The three-dimensional data sets  $v(x, y, t)$  and  $I(x, y, t)$  of each line were then apodized with 10% cosine bells in all three dimensions, and three-dimensional Fourier transforms  $T_v(k_x, k_y, \omega)$  and  $T_I(k_x, k_y, \omega)$  were computed with standard FFT routines. By integrating the power  $T_a T_a^*$  and (complex) crosspower spectra  $T_a T_b^*$  in azimuth in the  $k_x - k_y$  plane, we derived  $k - \omega$  power  $P_a$ , phase difference  $\Phi_{ab}$  and coherence

spectra  $C_{ab}$  – where  $a, b$  stand for the velocity or for the intensity signal observed in a certain spectral line:

$$P_a(k_h, \omega) = \sum_{k_x^2 + k_y^2 = k_h^2} T_a T_a^*(k_x, k_y, \omega) \quad (2)$$

$$\Phi_{ab}(k_h, \omega) = \arg \left\{ \sum_{k_x^2 + k_y^2 = k_h^2} T_a T_b^*(k_x, k_y, \omega) \right\} \quad (3)$$

$$C_{ab}(k_h, \omega) = \frac{\left| \sum_{k_x^2 + k_y^2 = k_h^2} T_a T_b^*(k_x, k_y, \omega) \right|}{\sum_{k_x^2 + k_y^2 = k_h^2} |T_a T_b^*(k_x, k_y, \omega)|} \quad (4)$$

Finally, the spatial components of all power spectra were corrected for the effects of *blurring* by atmospheric seeing with the help of the mean *modulation transfer function* (MTF) of short exposure images, given by Fried's (1966) equation

$$\text{MTF}(u) = \text{MTF}_{\text{tel.}} \cdot e^{\left( -3.44 \left( \frac{D}{r_0} \right)^{5/3} u^{5/3} (1 - u^{1/3}) \right)}, \quad (5)$$

as a function of the above mentioned parameter  $r_0$ , where

$$\text{MTF}_{\text{tel.}} = \frac{2}{\pi} \left( \arccos(u) - u \sqrt{1 - u^2} \right) \quad (6)$$

is the diffraction limited MTF and  $u = k_h \cdot \frac{\lambda f}{D}$  is the normalized spatial frequency. Using this notation, we can write the corrected power spectrum as

$$P(u) = \frac{P_{\text{obs.}}(u)}{\text{MTF}^2(u)}. \quad (7)$$

## 3. Results and discussion

### 3.1. Power spectra

We first discuss spatial and spatio-temporal power spectra which can be directly compared with the results presented in Paper I. In order to investigate the convective part of the signals we have to remove non-convective phenomena like the p-modes by applying a subsonic filter in the Fourier domain. In case of the white light images, the best 100 images (i.e. those with highest intensity contrast) have been selected after filtering, and the mean spatial power has been calculated as described in Sect. 2 (see Eq. 1).

On the other hand, spatial power spectra of the intensity and velocity signals of both Fraunhofer lines have been obtained from the  $k - \omega$  power spectra defined in Eq. (2) by integrating over all temporal frequencies  $\nu$ . In this step the frequencies above the Lamb mode ( $\omega = c_s k_h$ ) corresponding to the oscillation part of the signal have been excluded.

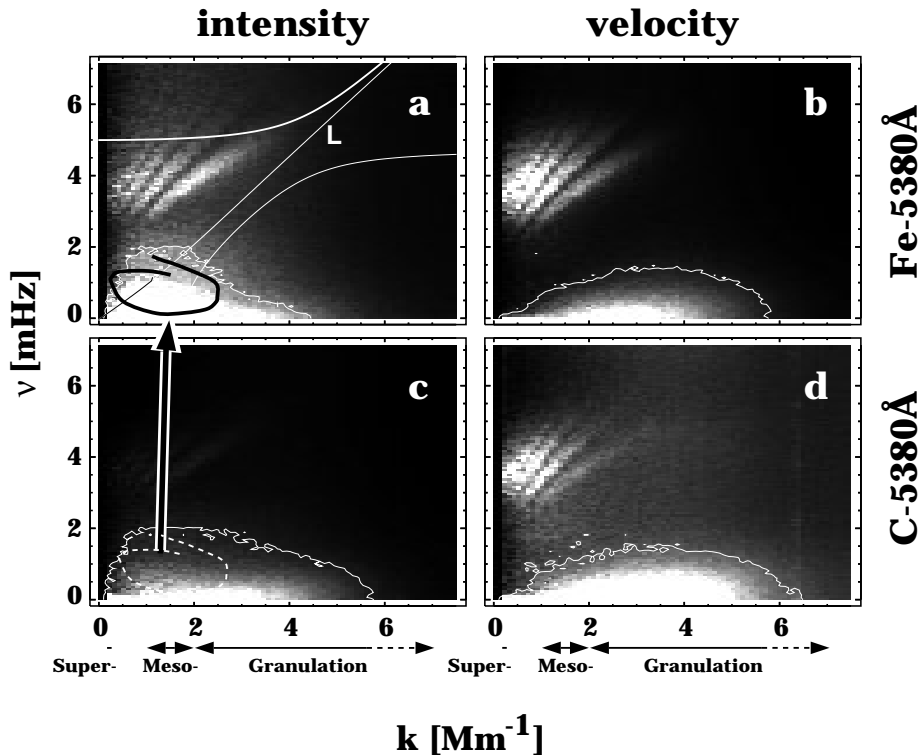


**Fig. 4a–d.**  $k - \omega$  power spectra of the  $v$  (right column) and  $I$  (left column) signals observed in the cores of the C-5380 (bottom row) and Fe-5380 (top row) absorption lines. The power is represented by linear grey scales. In both the intensity (a+c) and the velocity (b+d) the same greyscale encoding is used at both levels in the photosphere. The approximate formation heights of the signals are 200 km (a), 260 km (b), 30 km (c) and 60 km (d) above  $\tau_{5000} = 1$  (see Table 1). The Fe-5380 contour level is increased by a factor of 5 in  $I$  (a with respect to c), and decreased by a factor of approx. 3 in  $v$  (b with respect to d). Further, the top left spectrum is projected against the characteristic frequencies of the diagnostic diagram, and the position of the power enhancement discussed in the text is marked.

Figure 3 summarizes the spatial power spectra of different signals. Common definitions for the spatial ranges of the three convective regimes – granulation, “mesogranulation” and supergranulation – are marked on the wavenumber axis.

The power spectrum of the best white light images, labeled  $I_{\text{cont}}$ , reveals, as do most of the other power spectra shown in Fig. 3, a single, broad distribution of granular and mesogranular sizes reaching its maximum at  $k_h \approx 3 \dots 4 \text{ Mm}^{-1}$ . This is in good agreement with the results in Paper I, even though, we again emphasize, they were based on a totally different observation technique. Besides simple offsets in the absolute power at different heights of formation, the only really different spatial power spectrum is that derived from the intensity measured in the core of the Fe-5380 line (originating from about 200 km above  $\tau_{5000} = 1$ ). Here, the maximum is shifted toward lower wavenumbers due to a power “enhancement” at mesoscales as indicated by the hatched region in Fig. 3.

Is it possible, with only the help of the power spectra, to identify further the nature of this mesoscale power? We find a first indication in the corresponding spatio-temporal power spectra shown in Fig. 4. Both, the intensity and the velocity  $k - \omega$  power spectra are represented by the same greyscale encoding at both formation heights. Comparing the two diagrams on the left side of Fig. 4 we can identify the position of the power “enhancement” at the medium wavenumber, medium frequency region indicated. Therefore, the first doubts about a relation to the “mesogranulation” phenomenon arise from this position as we would expect the maximum power near the zero frequency of a 4 hour time series. Further, a comparison of the lines of equal power, like the examples projected in Fig. 4, suggests the different  $I$  power spectrum at the higher level is caused by the

obvious lack of power at high wavenumbers rather than by a real power “enhancement” of the mesoscales.

The identification of the dynamical process responsible for this mesoscale power reaching the higher level while the main granular signal is suppressed requires a full dynamical study of the velocity and intensity fluctuations with the help of  $k - \omega$  phase spectra as discussed in the following section.

### 3.2. Phase difference spectra

The phase difference spectra are summarized in Fig. 5, projected against the characteristic frequencies of the  $k - \omega$  diagram as shown in Fig. 5a, or with overlaying contours of the corresponding coherence as in Fig. 5b–j. The  $\Phi_{v-I}$  phase difference spectra measure the delay between the signals of the vertical velocity and the intensity, defined positive for leading velocity. They show at the C I-5380 line levels (Fig. 5h–j) for all low frequencies a vanishing phase difference, as one might expect for convective signals, and high coherence values at spatial wavenumbers around  $k_h \approx 2 \dots 4 \text{ Mm}^{-1}$ . Instead, the positive (red) phase difference at approximately 2 mHz is caused by an oscillation signal as first stated by Deubner (1990).

Looking at higher atmospheric levels (Fig. 5d–g, approx. 200 km as indicated in Table 1), the  $\Phi_{v-I}$  spectra show generally a higher coherence. This might be a consequence of the higher S/N ratio of the observations in the stronger Fe I-5380 line. In the phase difference spectrum corresponding to the lowest atmospheric height observed in the Fe I-5380 line (Fig. 5d), we find coherence values over 0.95 in the low frequency range at spatial wavenumbers between  $k_h \approx 2 \dots 6 \text{ Mm}^{-1}$ , and vanishing (white) or slightly negative (light blue) phase values. With in-

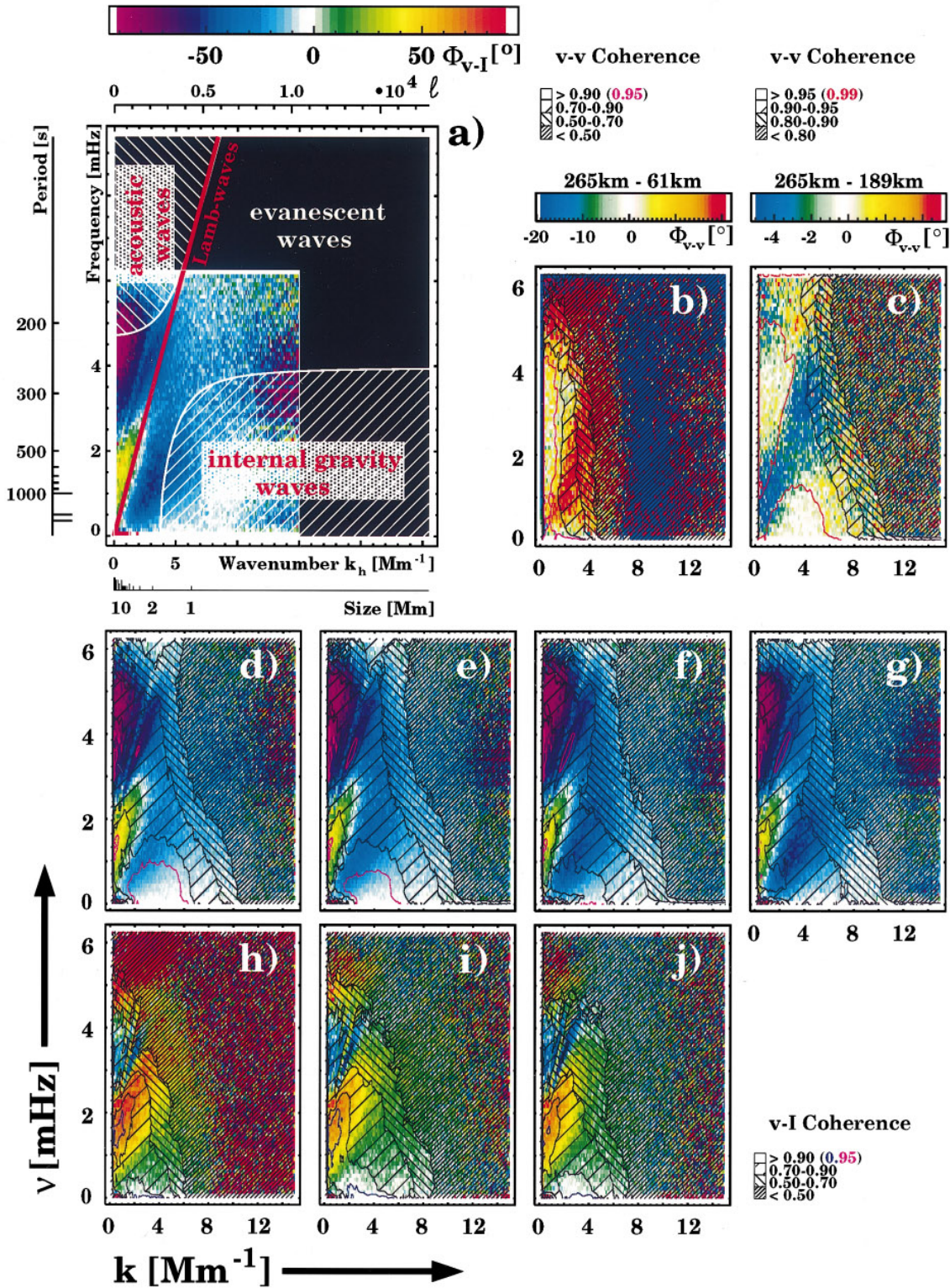


**Fig. 5a-j.** Summary of the phase difference spectra, **a** as projected against the characteristic frequencies of an isothermal atmosphere with  $c_s = 7000 \text{ m s}^{-1}$  and  $\tau_R = 30 \text{ s}$ ; **b-j** with contours representing the coherence (the smallest spacing of the hatch lines indicates the lowest coherence values): The phase difference spectra  $\Phi_{v-v}$  between velocity signals at different heights (**b-c**) reveal the vertical phase propagation (red indicates upward, blue downward propagation). The phase difference spectra  $\Phi_{v-I}$  between velocity and intensity fluctuations at the same level (**d-j**) cover 3 levels in the C I-5380 line (*bottom row, h-j*) and 4 levels in the Fe I-5380 line (*central row, d-g*, with increasing height corresponding to the sequence h-i-j-d-e-f-g (see Table 1).

creasing formation height, this region shrinks and shifts toward lower spatial wavenumbers, indicating finally a highly coherent signal with a significant negative phase of about  $\Phi_{v-I} \approx -40^\circ$  in Fig. 5g, which corresponds roughly to the region of “enhanced” power mentioned in the previous section. So, the physical phenomenon related to this mesoscale power should be of some different nature than convection. A possible interpretation of negative  $\Phi_{v-I}$  phase values in the region below the Lamb mode as internal gravity waves has been made by other authors (e.g. Deubner et al. 1992) and can be found in one-dimensional models of this oscillation type (Mihalas & Toomre 1981). Our  $\Phi_{v-I}$  phase difference spectra, for the first time, indicate such a negative phase signal as related to a mesoscale phenomenon.

The Figures 5b,c show the  $\Phi_{v-v}$  phase difference spectra between velocity signals at different heights in the solar atmosphere. In our case, the observational technique introduces a time delay between the C I and the Fe I data as the latter is scanned approximately 40 s after the first. The corresponding phase difference, a linear function of the frequency  $\omega$ , has been subtracted from the  $k - \omega$  phase difference determined as indicated in Eq. (4).

A positive difference indicates the signal at the lower level to lead (i.e. upward propagation). We find a generally low coherence between the velocity signals in the Fe I-5380 line and the C I-5380 (see Fig. 5b). Only large scale structures in the velocity signals at such different heights are well correlated, indicating a general upward propagation. Obviously, small scale vertical flows do not essentially propagate to levels as high as 250 km (cf. Komm et al. 1991). Instead, a comparison of the velocity signals at two less different heights (Fig. 5c) reveals a downward propagation for signals near the Lamb mode including the region of negative  $\Phi_{v-I}$  phase discussed above, while structures with smaller spatial scales still show an upward propagation. A downward phase propagation is to be expected in the case of internal gravity waves (see e.g. Schwartz & Stein 1975).

So, both, the  $\Phi_{v-I}$  and the  $\Phi_{v-v}$  phase difference spectra indicate a regime of internal gravity waves to be related with the medium frequency mesoscale structures present at heights about 200 km in the photosphere.

### 3.3. Fourier filtered time series

We can now use the  $\Phi_{v-I}$  phase difference to define a filter to distinguish further the subsonic signals in the spatio-temporal domain. We therefore apply first a subsonic Fourier filter to the 3D Fourier transform of the velocity signal in the Fe I-5380 line core, to remove the pressure driven oscillatory part. We then construct an axisymmetrical filter defined by the smoothed contour line  $\Phi_{v-I}^{\text{Fe } 5380, \text{core}} = -30^\circ$  (see Fig. 6) as dividing line between the low frequency convective and oscillatory parts. The filter function vanishes smoothly, like cosine bells, on this dividing contour line, in order to avoid aliasing. Inverse Fourier transformation of both complementary parts of the Fourier transform, the negative phase oscillatory part inside the torus shown in Fig. 6 and the outlying convective part, reveals the corresponding signals in the space–time domain. Both are represented in

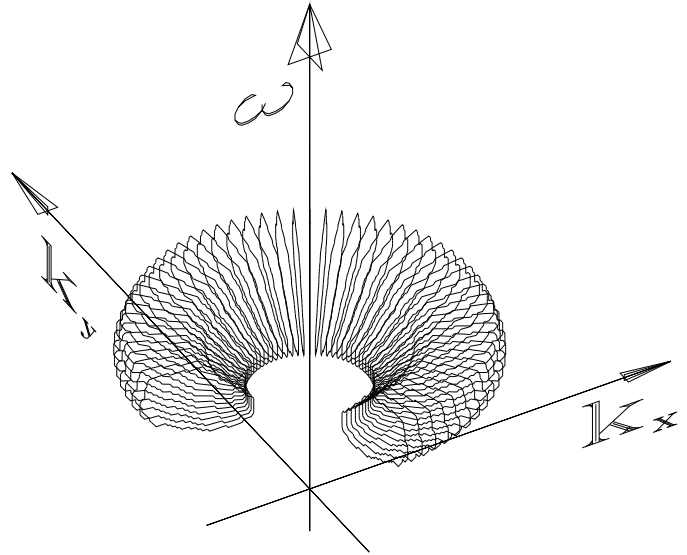


**Fig. 6.** The filter function used to distinguish the convective from the non convective signals in the Fe I-5380. Rotation of the contour line  $\Phi_{v-I} = -30^\circ$  of the phase spectrum in Fig. 5g around the frequency axis of the 3D Fourier space defines the torus surface where the filter smoothly drops to zero.

Fig. 7 by time slices, cutting the 3D velocity data cube at the same spatial position. This filter procedure has been applied only to the first 2.5 hours of observations.

Together, both time slices demonstrate clearly the different dynamical processes causing the two signals of different  $\Phi_{v-I}$  phase. The left slice of Fig. 7, representing the convective regime with vanishing  $\Phi_{v-I}$  phase difference, is dominated by the long term structures of the granulation and the supergranulation. Some of the granular structures can be followed at nearly the same spatial position for up to 40 minutes. Near the spatial position labeled 60'' we find a supergranular boundary, stable over the whole period.

Instead, the slice on the right side shows a totally different behaviour. Here, the structures corresponding to the domain of negative  $\Phi_{v-I}$  phase vary more rapidly with medium periods of about 10 minutes. A rapid horizontal propagation of several  $\text{km s}^{-1}$  makes the patterns of upward (white) and downward (black) flows appear like a ship’s wake. One might expect this high horizontal phase propagation – too high for being interpreted by convective flows – for internal gravity waves which should propagate rather horizontally in the solar atmosphere. So, the filtered time slices are a further indication of the presence of internal gravity waves with meso scales at about 200 km in photosphere.

## 4. Conclusions

We investigate a long term, two-dimensional spectral time series obtained with the UBF and FP tunable filter device at the VTT of the Sac Peak Observatory. The main goal of this observation is

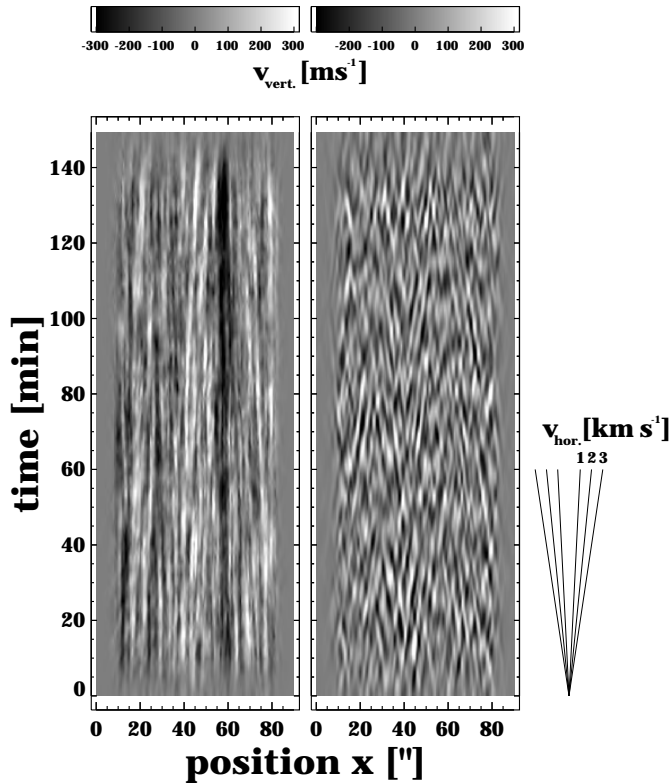


**Fig. 7.** Time slices of the two complementary velocity signals below the Lamb mode with different  $\Phi_{v-I}$  phase values in the Fe I-5380 line at approx. 200 km in the photosphere. The slices are the results of the inverse Fourier transform of the subsonic region in the  $k - \omega$  diagram after applying the complementary filters defined by the torus shown in Fig. 6, and show the vertical velocity. The *right* slice corresponds to the negative phase signal inside the torus, the *left* slice shows the outlying convective signal. The horizontal propagation of the patterns of upward (white) and downward (black) motion in the right panel can be determined by their spatial shifts as a function of time as indicated by the labels on the right.

to determine *simultaneously* the vertical *and* horizontal velocity of low frequency flows in the solar photosphere *by a single set of observations*, in order to address the disagreement between spectroscopic investigations of the vertical velocity and the results of measurements of the horizontal velocity of convective flows based on the local correlation tracking algorithm.

We use, therefore, a time series composed of wavelength scans taken with the tunable filter to determine the vertical velocity at different heights in the photosphere, similar to the spectroscopic investigation in paper I, but extended to higher spatial wavenumbers. This part is discussed in the present paper. Furthermore, we use the simultaneously taken white light time series to calculate the horizontal velocity of quasi-stationary flows in the low photosphere. This part will be discussed in an forthcoming paper.

The Fourier analysis of the spectral time series confirmed a number of results obtained in previous works. Spatial power

spectra of the subsonic part of the signal show a bimodal structure. The broad distribution of granular sizes with an absolute maximum at  $k_h \approx 3 \dots 4 \text{ Mm}^{-1}$  (see Fig. 3), in accordance with previously published high resolution spectra (e.g. Deubner & Mattig 1975; Ricort & Aime 1979; Schmidt et al. 1981; von der Lühe & Dunn 1987; Collados & Vazques 1987), does not support the hypothesis of a turbulent cascade of convective motions (cf. Zahn 1987). A separate regime of “mesogranulation” distinct from granulation by a power gap has *not* been found.

When the  $k - \omega$  phase difference spectra are taken into account, the general picture of the dynamics in the photosphere drawn by Deubner et al. 1992 is confirmed. In fact, apart from the p-modes, three different regimes can be found in the  $k - \omega$  plane: in the “plateau” regime (1) above the Lamb mode at about 2 mHz the velocity leads the intensity signal by some  $50^\circ$ . At the Lamb mode the  $\Phi_{v-I}$  phase drops towards vanishing phase values (2) in case of low photospheric levels and negative values (3) in case of higher levels. So, the slow quasi-stationary flows are driven by convection at low levels, and generates gravity waves at higher levels (cf. Durrant & Nesis 1981). Only the flows at large supergranular scales show an anticorrelation between velocity and intensity fluctuations ( $\Phi_{v-I} \approx 180^\circ$ ) in the entire range of heights investigated by our observations. This interesting detail emphasizes, at least partly, a non convective character of supergranulation, as the bright network caused by enhanced dissipation in magnetic fields may be.

In addition to this known scenario, a fourth phase regime at the higher levels has been found with vanishing  $\Phi_{v-I}$  phase (4), which limits the negative phase regime of internal gravity waves (3) to a wedge-of-cake like region below the Lamb mode pointing towards medium spatial and medium temporal frequencies (see Fig. 5g), where the power of the intensity fluctuations is enhanced and the velocity and intensity signals are highly coherent. So, the signal of gravity waves in the photosphere seems to be somewhat related to mesoscales, as also the downward phase propagation (negative  $\Phi_{v-v}$  phase values) is limited to low wavenumbers. The inverse Fourier transform of only this negative phase signal (3) reveals a new, even more convincing, argument for gravity waves as the source of the subsonic phenomena at higher levels: the significant horizontal propagation character of this phenomenon (Fig. 7).

On the other hand, the new phase regime (4) limiting the internal gravity wave signal at high wavenumbers merits further theoretical and observational investigation. In contrast to the signal of internal gravity waves (3), it shows no substantial horizontal propagation. This seems to indicate that there is still a convective character at such heights (approx. 200 km) in the photosphere.

As a consequence of the above demonstrated superposition of the different dynamical phenomena (3 and 4) in the region below the Lamb mode, a simple subsonic filter cannot sufficiently remove *all* oscillatory parts for an investigation of convective intensity or velocity fluctuations. Instead, a full dynamical study must be provided, in order to fully distinguish the oscillatory and the convective signals.

*Acknowledgements.* This work is based on the Ph.D. thesis of Th. Straus written at the Dipartimento di Astronomia e Scienze dello Spazio, Università di Firenze. Th. S. gratefully acknowledges the staff of observers at the VTT of the SacPeak Observatory for the professional collaboration and the always friendly environment during the observation. He also wishes to thank F.-L. Deubner, P. Brandt and G. Severino for stimulating discussions, and G. Cauzzi and K. Reardon for proofreading the manuscript.

## References

- Bendlin C., Volkmer R., 1993, *A&A* 278, 601  
 Bonaccini D., Stauffer F., 1990, *A&A* 229, 272  
 Bonaccini D., Righini A., Cavallini F., Ceppatelli G., 1989, *A&A* 217, 368  
 Brandt P. N., Mauter H. A., Smartt R., 1987, *A&A* 188, 163  
 Brandt P. N., Ferguson S., Scharmer G. B. et al., 1991, *A&A* 241, 219  
 Caccin B., Gomez M. T., Marmolino C., Severino G., 1977, *A&A* 54, 227  
 Chan K. L., Nordlund Å., Steffen M., Stein R. F., 1991, in: *Solar interior and atmosphere*, Cox A., Livingston W., Matthews M. (eds), IAU, part 1, pp. 223–274  
 Collados M., Vázquez M., 1987, *A&A* 180, 223  
 Chou D. Y., Labonte B. J., Braun D. C., Duvall T. L., 1991, *ApJ* 372, 314  
 Deubner F.-L., 1975, *A&A* 44, 371  
 Deubner F.-L., 1989, *A&A* 216, 259  
 Deubner F.-L., 1990, in: *Solar Photosphere: Structure, Convection, and Magnetic Fields*, Stenflo J. O. (ed.), IAU Symp. 138, p. 217  
 Deubner F.-L., Fleck B., 1989, *A&A* 213, 423  
 Deubner F.-L., Mattig W., 1975, *A&A* 45, 167  
 Deubner F.-L., Fleck B., Schmitz F., Straus Th., 1992, *A&A* 266, 560  
 Durrant C. J., Nesis A., 1981, *A&A* 95, 221  
 Fried D. L., 1966, *J. opt. Soc. Am.* 56, 1372.  
 Hathaway D.H., Rhodes E.J., Cacciani A., Korzennik S.G., 1991, in: *Challenges to Theories of the Structure of Moderate Mass Stars*, Gough D. O., Toomre J. (eds.), *Lecture Notes in Physics* 388, p. 163  
 Johannesson A., Bida T., Lites B., Scharmer G. B., 1992, *A&A* 258, 572  
 Ginet G. P., Simon G. W., 1992, *ApJ* 386, 359  
 Komm R., Mattig W., Nesis A., 1991, *A&A* 252, 827  
 Leibacher J. W., Stein R. F., 1971, *Astrophys. Letters* 7, 191  
 Marmolino C., 1995, private communication  
 Marmolino C., Severino G., 1991, *A&A* 242, 271  
 Marmolino C., Severino G., Deubner F. L., Fleck B., 1993, *A&A* 278, 617  
 Mein P., 1991, *A&A* 248, 669  
 Mihalas B. W., Toomre J., 1981, *ApJ* 249, 349  
 Nordlund Å., Stein R. F., 1995, in: *Stellar Evolution: What Should Be Done*, 32<sup>nd</sup> Liège Int. Astroph. Coll.  
 November L. J., 1989, in: *High Spatial Resolution Solar Observations*, von der Lühse O. (ed.), *Sunspot*, N.M., p. 457  
 November L. J., Simon G. W., 1988, *ApJ* 333, 427  
 November L. J., Toomre J., Gebbie K. B., Simon G. W., 1981, *ApJ* 245, L123  
 November L. J., Simon G. W., Tarbell T. D., Title A. M., Ferguson S. H., 1987, in: *Theoretical Problems in High Resolution Solar Physics*, NASA-Goddard Space Flight Center, p. 121  
 Noyes R. W., 1967, in: *Aerodynamic Phenomena in Stellar Atmospheres*, Thomas R. N. (ed.), Academic Press, New York, p. 293  
 Ricort G., Aime C., 1979, *A&A* 14, 167  
 Schmidt W., Knölker M., Schröter E.-H., 1981, *Solar Phys.* 73, 217  
 Schwartz R. A., Stein R. F., 1975, *ApJ* 200, 499  
 Simon G., Leighton R. B., 1964, *ApJ* 140, 1120  
 Simon G. W., Title A. M., Topka K. P., Tarbell T. D., Shine R. A., 1988, *ApJ* 327, 964  
 Stein R. F., Nordlund Å., 1989, *ApJ* 342, L95  
 Straus Th., 1991, *Dipl. Thesis* (Würzburg)  
 Straus Th., Deubner F.-L., Fleck B., 1992, *A&A* 256, 652  
 Ulrich R. K., 1970, *ApJ* 162, 993  
 von der Lühse O., Dunn R. B., 1987, *A&A* 177, 265  
 Wang Z., Ulrich R. K., Coroniti F. V., 1995, *ApJ* 444, 879  
 Zahn J.-P., 1987, in: *Solar and Stellar Physics*, Schröter E.-H., Schüssler M. (eds.), *Lecture Notes in Physics* 292, p. 55

This article was processed by the author using Springer-Verlag  $\text{\TeX}$  A&A macro package 1992.